Hot-phonon-assisted resonant tunneling in a quantum well

P. Král,* F. W. Sheard, and F. F. Ouali
Department of Physics, University of Nottingham, Nottingham NG7 2RD, United Kingdom
(Received 30 September 1997; revised manuscript received 15 January 1998)

We theoretically investigate dc electron resonant tunneling through an impurity state in a quantum well assisted by hot acoustical phonons. Numerical results for the tunneling current, obtained by nonequilibrium Green functions, reflect the hot-phonon-induced change in the spectrum and population of the impurity state. The induced change of the *I-V* characteristics has a typical two-peak form, which for larger populations of the level becomes distorted by increased *intralevel phonon emissions*. A qualitative agreement with experiments is obtained. [S0163-1829(98)04224-6]

I. INTRODUCTION

Hot acoustic phonons form a new tool in experimental investigations of structural and transport properties of low-dimensional semiconductor systems.[1–5] In these studies often the transfer of a phonon momentum plays a key role, but the transfer of a phonon energy is sufficient for observations of the (equilibrium LO) phonon-assisted resonant tunneling.[6] These measurements raised the idea that resonant tunneling could be used as a generator and detector of hot acoustical phonons.[7] The detection experiments were first realized in undoped and Si δ-doped quantum wells,[8,9] where the resonant current occurred through the impurity level in the well. The hot phonons induce broadening of the resonant *I-V*. The subtracted change of the *I-V* has two peaks, attributed to assisted tunneling as a result of phonon absorption and emission, but the large peak separation seemed to contradict the very small transferred phonon energy.

Here we model this nonlinear system with competing parameters and describe its dynamics by nonequilibrium Green functions (NGF).[10,11] The Kadanoff-Baym transport equations for electron correlation functions at the impurity are numerically solved in the presence of dc bias and hot phonons.[12–18] From their solution the nonequilibrium spectrum and population of the level are obtained. They enter the expression for the resonant tunneling current through the impurity, which is arranged to a form with clearly separated injection and relaxation parts [see Eq. (23)].

Several limits can be pointed out in the results obtained. Low energy phonons, with energies smaller than the level width (either homogeneous or inhomogeneous), increase broadening of the level and the tunneling can be considered as quasielastic. At higher phonon energies, absorption and emission satellites form on either side of the level or the resonances of the well.[19] In both frequency regimes two peaks are also seen in the tunneling current; they are symmetrically placed around the resonance, if coupling of the level to the emitter is weak (low populations). For stronger coupling to the emitter, the level becomes narrowed as the emitter sweeps up. The increased density of final states enhances relaxation of electrons on the level, stimulated by hot phonons, and destroys the symmetry of the response current. Studies with monochromatic phonons reveal a cutoff in the excitation spectrum, due to the confinement of the level in the well, which is less visible in the response for hot-phonon excitations. Heating of the contact Fermi seas by the hot phonons is also investigated and the relevance of our results for the available experiments is discussed.[20]

The paper is organized as follows. In Sec. II the model system is introduced and its parameters are determined. In Sec. III we derive the nonlinear and linearized transport equations in the presence of hot phonons. An improved formula for the resonant tunneling current is also obtained here. In Sec. IV numerical examples are presented and discussed in detail for several configurations of the system, including different values of Fermi energy in the emitter and hot-phonon temperatures.

II. THE MODEL

The model system[8] is formed by a double-barrier heterostructure with a donor level confined in the well between the two barriers. The reservoirs are connected via the barriers to the resonant level, where the electrons are coupled to bulk acoustic phonons. A sketch of the system is shown in Fig. 1.

This model is described by the following spinless Hamiltonian with the electron-phonon interaction:

$$H=\sum_{k;\alpha=L,R} E_{k,\alpha}c^{\dagger}_{k,\alpha}c_{k,\alpha}+E_0 d^{\dagger}d + \sum_{k;\alpha=L,R} \gamma_{k;\alpha}(c^{\dagger}_{k,\alpha}d+\text{H. c.}) + \sum_q \hbar\omega_q b^{\dagger}_q b_q+\sum_q F(q)M(q)d^{\dagger}d(b_q+b^{\dagger}_{-q}). \quad (1)$$

Here $c^{+}_{k,\alpha=L,R}(c_{k,\alpha=L,R})$ and $E_{k,\alpha=L,R}$ are creation (annihilation) operators and energies for electrons in the left (L) and right (R) reservoirs, $d^{\dagger}$ (d) and E_0 describe the same for the level and $\gamma_{k,\alpha=L,R}$ are the coupling parameters between the level and the reservoirs. The operators $b^{\dagger}_q(b_q)$ and energies $\hbar\omega_q$ (isotropic) describe acoustic phonons coupled by the interaction matrix elements $M(q)$ to the electrons on the level. The structure factor $F(q)$ is a square of the donor wave function transformed in a momentum representation.

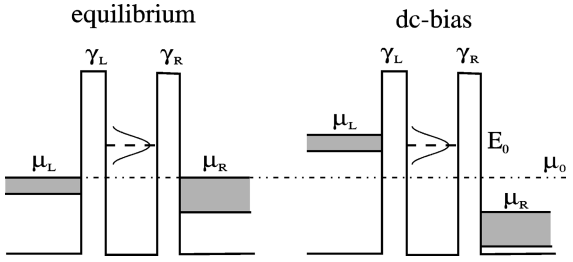

FIG. 1. A scheme of the resonant tunneling system. In equilibrium the chemical potentials in the reservoirs coincide, $\mu_L=\mu_R=\mu_0$. Under a dc bias they shift with the contact bands equal amounts but in opposite directions.

The donor wave function $\phi(r)$ of a diameter $\sigma=10$ nm (GaAs) is confined in the z direction of the well of the width $w=5$ nm and can be approximated as follows:[21]

$$\phi(r)=\sqrt{\frac{2}{\pi w}}\frac{1}{\sigma}e^{-(x^2+y^2)/2\sigma^2}\cos\left(\frac{\pi}{w}z\right)\left(-\frac{w}{2}<z<\frac{w}{2}\right), \tag{2}$$

with the structure factor

$$F(q)=\frac{2}{w}e^{-\sigma^2(q_x^2+q_y^2)/4}\left\{\frac{\sin[(w/2)q_z]}{q_z}+\frac{1}{2}\left[\frac{\sin[(w/2)q_z-\pi]}{q_z-2\pi/w}+\frac{\sin[(w/2)q_z+\pi]}{q_z+2\pi/w}\right]\right\}. \tag{3}$$

We apply a simple form for the electron-phonon matrix element[22] for a deformation potential and piezoelectric coupling[23] to the phonons

$$M(q)=\left(\frac{1}{2\rho_{\rm cryst}s|q|}\right)^{1/2}(D|q|+iM_{\rm piezo}),\quad \hbar\omega_q=\hbar s|q| \tag{4}$$

where the parameters used are the density $\rho_{\rm cryst}=5317$ kg/m^3, the sound velocity $s=5220$ m/s ($s_{\rm trans}=3000$ m/s), the deformation potential constant $D=11$ eV, and the piezoelectric constant $M_{\rm piezo}=1.2$ eV/nm. The numerical results show that for the present parameters and temperatures used both coupling mechanisms are approximately of the same strength (see also Ref. 24). In the following we limit for simplicity only to the deformation potential coupling to LA phonons.

III. NONLINEAR DESCRIPTION

We derive transport equations for electron correlation functions on the impurity level and relate their solution with the dc tunneling current.

A. NGF transport equations

The system is described by Green functions $G(1,2)$ time ordered along a contour in the complex plane[25] (see also the Appendix). Reduction to real times of the Dyson equation for $G(1,2)$ gives a set of Kadanoff-Baym (KB) equations[10] in the integral form[26] for the nonequilibrium correlation functions

$$G^<(\omega)=G^r(\omega)\Sigma^<(\omega)G^a(\omega),$$

$$G^>(\omega)=G^r(\omega)\Sigma^>(\omega)G^a(\omega). \tag{5}$$

These correlation functions have a matrix form $G^{<,>}_{i,j}(\omega)$, $i,j=L,R,w$ (left, right reservoir, well). Because scattering is present only in the well, the analysis can be limited to the well diagonal elements $G^{<,>}_{ww}(\omega)\equiv G^{<,>}(\omega)$.

The nonequilibrium electron propagator $G^r(\omega)$ on the level is

$$G^r(\omega)=\frac{1}{(G_0^r)^{-1}(\omega)-\Sigma_c^r(\omega)},$$

$$G_0^r(\omega)=\frac{1}{\hbar\omega-E_0-\Sigma_H^r-\Gamma_L^r(\omega)-\Gamma_R^r(\omega)}, \tag{6}$$

where $G_0^r(\omega)$ is the free propagator, $\Gamma^r_{L,R}(\omega)$ are the propagators for the coupling Green functions, and Σ_H^r, $\Sigma_c^r(\omega)$ are the propagators for the Hartree[17] and many-particle self-energy functions, describing the electron-phonon interaction. $G^{r,a}(\omega)$ can also be obtained from the nonequilibrium spectrum $A(\omega)=G^>(\omega)+G^<(\omega)$ as in Eqs. (A5) and (A6). The coupling terms give the *homogeneous* level broadening

$$\sigma_{\rm hom}\approx-{\rm Im}[\Gamma_L^r(E_0/\hbar)+\Gamma_R^r(E_0/\hbar)], \tag{7}$$

which can be strongly dependent on the dc bias.

The nonequilibrium correlation functions $\Sigma^{<,>}(\omega)$ for the self-energy in Eq. (5) are formed by the coupling functions $\Gamma^{<,>}_{L,R}(\omega)$ and the many-particle parts $\Sigma_c^{<,>}(\omega)$,

$$\Sigma^<(\omega)=\Gamma_L^<(\omega)+\Gamma_R^<(\omega)+\Sigma_c^<(\omega),$$

$$\Sigma^>(\omega)=\Gamma_L^>(\omega)+\Gamma_R^>(\omega)+\Sigma_c^>(\omega). \tag{8}$$

The correlation function for the Hartree part is zero $\Sigma_H^{<,>}=0$, as in electron-electron interactions. The coupling functions $\Gamma_{L,R}(\omega)$ can be expressed for the Hamiltonian in Eq. (1) as follows [$\Gamma^a_{L,R}(\omega)$, $\Gamma^>_{L,R}(\omega)$ are analogous]:

$$\Gamma^{r,<}_{L,R}(\omega)=\sum_k|\gamma_{k;L,R}|^2G^{r,<}_{L,R}(k,\omega)\approx|\gamma_{L,R}|^2\sum_k G^{r,<}_{L,R}(k,\omega)$$

$$=|\gamma_{L,R}|^2G^{r,<}_{L,R}(\omega), \tag{9}$$

where $G_{L,R}(\omega)$ are the local elements of the Green functions in the reservoirs. We assume that $\gamma_{k;L,R}$ depend weakly on k in the region of the filled emitter band with the Fermi energy $E_{F_L}\approx1$ meV, since the related momentum is much smaller than the in-plane momentum uncertainty from the impurity level $k_{F_L}=\sqrt{(2m_eE_{F_L})}/\hbar\approx0.053$ nm$^{-1}\ll2\pi/\sigma\approx0.6$ nm^{-1}. Therefore the momentum conservation (k dependence of $\gamma_{k;L,R}$) should not restrict much tunneling.

In experiments[8] the emitter (collector) is usually two-dimensional (2D) (3D) electron gas. In a small range of potentials, we can take both as 2D gases with a constant density of states.[27] The correlation functions $G^{<,>}_{L,R}(\omega)$ then result from these spectral functions (densities of states) $A_{L,R}(\omega)$ as follows:

$$A_{L,R}(\omega)=A^0_{L,R}[\Theta(\hbar\omega-E_{\text{top};L,R})-\Theta(\hbar\omega-E_{\text{bot};L,R})],$$

$$A^0_{L,R}=\frac{2\pi}{E_{\text{top};L,R}-E_{\text{bot};L,R}},$$

$$G^<_{L,R}(\omega)=A_{L,R}(\omega)n_{FD}(\hbar\omega-\mu_{L,R}),$$
$$G^>_{L,R}(\omega)=A_{L,R}(\omega)[1-n_{FD}(\hbar\omega-\mu_{L,R})]. \tag{10}$$

Here $E_{\text{bot};L,R}$ ($E_{\text{top};L,R}$) are the bottom (top) energies of the bands in the reservoirs, $\mu_{L,R}$ are the chemical potentials, hold as constant in the reservoirs. Under a dc bias, the contact bands shift by the same amount but in opposite directions with respect to the equilibrium chemical potential $\mu_0=0$ (i.e., $\mu_L=-\mu_R$) and the rigid position of the level E_0 (measured from μ_0). In equilibrium the bands are located at $E_{\text{bot};L}=-1$ meV, $E_{\text{bot};R}=-50$ meV, $E_{\text{top};L,R}=E_{\text{bot};L,R}+200$ meV.

We assume that the population $f_P(\omega)$ of the hot LA phonons varies slowly in time, so that the correlation functions for hot phonons can be written in a quasiequilibrium form (A4),

$$D^<(k,\omega)=A_P(k,\omega)f_P(\omega),$$
$$D^>(k,\omega)=A_P(k,\omega)[1+f_P(\omega)]. \tag{11}$$

Here the phonon spectral function $A_P(k,\omega)$ has the equilibrium form for 3D free phonons[22] (with explicit emission and absorption terms)

$$A_P(q,\omega)=2\pi[\delta(\hbar\omega-\hbar\omega_q)-\delta(\hbar\omega+\hbar\omega_q)]$$
$$=\frac{2\pi\omega}{\hbar s^2\sqrt{(\omega/s)^2-q_z^2}}\delta\left(|q_t|-\sqrt{\left(\frac{\omega}{s}\right)^2-q_z^2}\right)$$
$$\times\Theta\left[\left(\frac{\omega}{s}\right)^2-q_z^2\right], \tag{12}$$

where $|q_t|=\sqrt{q_x^2+q_y^2}$ is chosen as a new variable. The quasistationary phonon distribution $f_P(\omega)$ is simply modeled by a weighted function with two Bose-Einstein distributions n_{BE} for the sample with the temperature T and the beam of hot phonons with T_h,

$$f_P(\omega)=\frac{n_{\text{BE}}(\hbar\omega,T)+n_{\text{BE}}(\hbar\omega,T_h)}{2}. \tag{13}$$

In more detailed investigations, angular distribution of phonons[4,20] and other effects should be considered.

The Hartree term of the electron self-energy is

$$\Sigma^r_H=\int\frac{d^3\overline{q}}{(2\pi)^3}[F(\overline{q})M(\overline{q})]^2D^r(\overline{q},\omega=0)\int\frac{d\hbar\overline{\omega}}{2\pi}G^<(\overline{\omega}), \tag{14}$$

where D^r is the phonon propagator. In the present calculations it can be neglected, since it contributes very little, due to the small strength of the electron-phonon interaction with LA phonons $g=\Sigma_q[M(q)/\hbar\omega_q]^2$. For similar reasons, the Migdal approximation of the many-particle part of the self-energy Σ_c can be used,[28,29] which gives the correlation function

$$\Sigma^<_c(\omega)=\frac{1}{(2\pi)^4}\int d\hbar\overline{\omega}d^2\overline{q}_td\overline{q}_z[F(\overline{q})M(\overline{q})]^2$$
$$\times G^<(\omega-\overline{\omega})D^<(\overline{q},\overline{\omega})$$
$$=\int\frac{d\hbar\overline{\omega}}{2\pi}G^<(\omega-\overline{\omega})\mathcal{A}(\overline{\omega})f_P(\overline{\omega}),$$

$$q_t=(q_x,q_y). \tag{15}$$

The effective spectral distribution $\mathcal{A}(\omega)$ results, if Eqs. (11) and (12) are substituted in Eq. (15) and the integration over q_t is performed similarly as in quantum wires,[30]

$$\mathcal{A}(\omega)=\frac{2D^2\text{sgn}(\omega)}{s^2\rho}\left|\frac{\omega}{s}\right|^2\int\frac{dq_z}{2\pi}\left\{\frac{\sin[(w/2)q_z]}{wq_z}\right.$$
$$\left.+\frac{1}{2}\left[\frac{\sin[(w/2)q_z-\pi]}{wq_z-2\pi}+\frac{\sin[(w/2)q_z+\pi]}{wq_z+2\pi}\right]\right\}^2$$
$$\times\exp\left\{-\frac{\sigma^2}{2}\left[\left(\frac{\omega}{s}\right)^2-q_z^2\right]\right\}\Theta\left(\left(\frac{\omega}{s}\right)^2-q_z^2\right). \tag{16}$$

The expressions (6)–(16) close the KB equations (5).

B. Solution of the KB equations

In a steady state the solution of the KB equations (5) $G^<(\omega)$, $G^>(\omega)$ can be formally written in a quasiequilibrium form, analogous to that used for phonons in Eq. (11),

$$G^<(\omega)=A(\omega)f(\omega),\quad G^>(\omega)=A(\omega)[1-f(\omega)]. \tag{17}$$

Any pair of these nonequilibrium functions $G^<(\omega)$, $G^>(\omega)$, $A(\omega)$, $f(\omega)$ gives the complete description of the system.

In nonequilibrium the distribution function $f(\omega)$ differs from the Fermi-Dirac form already in the absence of interactions. In this trivial case it can be immediately written down when substituting the coupling functions $\Gamma^{<,>}_{L,R}$ from Eq. (9) into the free KB equations

$$G^{<,>}_0(\omega)=G^r_0(\omega)[\Gamma^{<,>}_L(\omega)+\Gamma^{<,>}_R(\omega)]G^a_0(\omega). \tag{18}$$

The free distribution function $f_0(\omega)$ results in a simple form

$$f_0(\omega)=\frac{\Gamma^<_L(\omega)+\Gamma^<_R(\omega)}{\Gamma^>_L(\omega)+\Gamma^<_L(\omega)+\Gamma^>_R(\omega)+\Gamma^<_R(\omega)}, \tag{19}$$

which is nonzero practically only in the energy region of the populated emitter band, where $\Gamma^<_L(\omega)\neq0$.

In the presence of interactions, the two contributions to $\Sigma^{<,>}(\omega)$ give a natural separation of the solution into elastic and inelastic components[12,13,16]

$$G_e^{<,>}(\omega)=G^r(\omega)[\Gamma_L^{<,>}(\omega)+\Gamma_R^{<,>}(\omega)]G^a(\omega),$$
$$G_i^{<,>}(\omega)=G^r(\omega)\Sigma_c^{<,>}(\omega)G^a(\omega),$$
$$G^{<,>}(\omega)=G_e^{<,>}(\omega)+G_i^{<,>}(\omega). \tag{20}$$

The free solution $G_0^{<,>}(\omega)$ in Eq. (18) is different from this elastic solution $G_e^{<,>}(\omega)$, which includes virtual phonon tunneling processes through the full propagators $G^{r,a}(\omega)$. The inelastic solution $G_i^{<,>}(\omega)$ includes all real phonon scattering processes.

C. Evaluation of the dc current

The dc current from the left (right) contact to the impurity level[31] is determined by its nonequilibrium spectrum and population, $A(\omega)$ and $G^<(\omega)[f(\omega)]$, as follows:

$$J_{L,R}=e\int\frac{d\bar{\omega}}{2\pi}|\gamma_{L,R}|^2[G_{L,R}^<(\bar{\omega})A(\bar{\omega})-A_{L,R}(\bar{\omega})G^<(\bar{\omega})],$$
$$=e\int\frac{d\bar{\omega}}{2\pi}|\gamma_{L,R}|^2A_{L,R}(\bar{\omega})\;\;A(\bar{\omega})$$
$$\times[n_F(\hbar\bar{\omega}-\mu_{L,R})-f(\bar{\omega})]. \tag{21}$$

In a steady state this common dc current is also equal to

$$J=\frac{J_L-J_R}{2}=\frac{e}{2}\int\frac{d\bar{\omega}}{2\pi}\{[\Gamma_L^<(\bar{\omega})-\Gamma_R^<(\bar{\omega})]A(\bar{\omega})$$
$$-[\Gamma_L^>(\bar{\omega})+\Gamma_L^<(\bar{\omega})-\Gamma_R^>(\bar{\omega})-\Gamma_R^<(\bar{\omega})]G^<(\bar{\omega})\}. \tag{22}$$

Substitution of $G^<(\omega)$ and $A(\omega)$ by the elastic and inelastic functions, resulting from Eq. (20), gives the elastic and inelastic currents $J_{e,i}$.

It would be convenient if the second term in Eq. (22), with the level population, was canceled out by a different choice of coefficients mixing $J_{L,R}$. For constant densities of states and $A_L^0=A_R^0=A^0$ the proper choice gives [collector population in $\Gamma_R^<(\bar{\omega})$ is neglected]

$$J=\frac{|\gamma_R|^2J_L-|\gamma_L|^2J_R}{|\gamma_L|^2+|\gamma_R|^2}$$
$$=\frac{eA_0|\gamma_L|^2|\gamma_R|^2}{|\gamma_L|^2+|\gamma_R|^2}\left(\int_{E_{\mathrm{bot};L}}^{E_{\mathrm{top};L}}\frac{d\bar{\omega}}{2\pi}A(\bar{\omega})n_{FD}(\hbar\bar{\omega}-\mu_L)\right.$$
$$\left.+\int_{E_{\mathrm{bot};R}}^{E_{\mathrm{bot};L}}\frac{d\bar{\omega}}{2\pi}A(\bar{\omega})f(\bar{\omega})\right). \tag{23}$$

This expression generalizes transmissivity formulas of the Landauer type.[32–34] In Eq. (23) the integration is divided into two regions, where different distributions are transferred through the level spectrum $A(\omega)$. In the injection region, limited by $E_{\mathrm{bot};L}$, electrons with the emitter distribution $n_{FD}(\hbar\omega-\mu_L)$ are transferred. In the region below $E_{\mathrm{bot};L}$, relaxed electrons *on the level*, described by $f(\omega)$, are transferred. Therefore the second term is nonzero only in the presence of interactions, when the emitter distribution is effectively broadened by inelastic scattering below the injection region. This term and part of the first term in Eq. (23), determined by the inelastic part of the spectrum broadening $A_i(\omega)=|G^r(\omega)|^2[\Sigma_c^<(\omega)+\Sigma_c^>(\omega)]$, contribute to the inelastic current J_i.

IV. LINEAR *phono* RESPONSE

Excitation by monochromatic phonons with frequency ω_0 can give valuable information about the present system. The response can be obtained from the full KB equations (5) or their linearized form with respect to the change of the hot-phonon distribution (13)

$$f_P(\omega)=n_{\mathrm{BE}}(\hbar\omega,T)+\delta f(\omega_0). \tag{24}$$

For small perturbations the approaches are identical. The nonlinear solution of the KB equations (5) can be expanded in a Taylor series in terms of the change $\delta f(\omega_0)$ as follows:

$$G^<(\omega)=G_n^<(\omega)+\frac{\delta G^<(\omega)}{\delta f(\omega_0)}\delta f(\omega_0)$$
$$+\frac{1}{2!}\frac{\delta^2G^<(\omega)}{[\delta f(\omega_0)]^2}[\delta f(\omega_0)]^2+\cdots, \tag{25}$$

where $G_n^<(\omega)$ is the solution in the presence of the dc bias but in the absence of $\delta f(\omega_0)$. The explicit form of the coefficients in Eq. (25) can be obtained if the functional derivatives are performed term by term directly in the KB equations (5).

For the linear term the following system of equations in a frequency representation can be obtained [equation for $\delta G^>(\omega)/\delta f(\omega_0)$ is analogous],

$$\frac{\delta G^<(\omega)}{\delta f(\omega_0)}=G_n^r(\omega)\frac{\delta\Sigma^r(\omega)}{\delta f(\omega_0)}G_n^<(\omega)+G_n^<(\omega)\frac{\delta\Sigma^a(\omega)}{\delta f(\omega_0)}G_n^a(\omega)$$
$$+G_n^r(\omega)\frac{\delta\Sigma^<(\omega)}{\delta f(\omega_0)}G_n^a(\omega). \tag{26}$$

In Eq. (26) the differential change of $G^r(\omega)$ was substituted by

$$\frac{\delta G^r(\omega)}{\delta f(\omega_0)}=G_n^r(\omega)\frac{\delta\Sigma^r(\omega)}{\delta f(\omega_0)}G_n^r(\omega). \tag{27}$$

The explicit nonvertex terms of a coherent origin are absent in Eqs. (26) and (27) and the Green functions are not explicitly shifted with the frequency ω_0 of the populated phonon mode as in the coherent field excitation.[30]

The transport equations (26) can be closed, if $\delta\Sigma^{<,>,r,a}(\omega)/\delta f(\omega_0)$ are expressed in terms of $\delta G^{<,>}(\omega)/\delta f(\omega_0)$. Self-consistent equations conserving physical laws[36] result only if the one-particle approximations of the self-energy become preserved also in the two-particle picture with the functional derivative (see also Ref. 30). This means to preserve in $\delta\Sigma^{<,>,r,a}(\omega)/\delta f(\omega_0)$ the Hartree term (14) and the many-particle term in the Migdal approximation (15). The linearized Hartree term is

$$\frac{\delta\Sigma_H^{r,a}}{\delta f(\omega_0)} = \int \frac{d^3\bar{q}}{(2\pi)^3}[F(\bar{q})M(\bar{q})]^2 D^{r,a}(\bar{q},\omega=0) \times \int \frac{d\hbar\bar{\omega}}{2\pi}\frac{\delta G^<(\bar{\omega})}{\delta f(\omega_0)}. \quad (28)$$

The linearized many-particle terms for the Migdal self-energy result as

$$\frac{\delta\Sigma_c^<(\omega)}{\delta f(\omega_0)} = \int \frac{d\hbar\bar{\omega}}{2\pi}\mathcal{A}(\bar{\omega})\left(G_n^<(\omega-\bar{\omega})\frac{\delta f(\bar{\omega})}{\delta f(\omega_0)} + \frac{\delta G^<(\omega-\bar{\omega})}{\delta f(\omega_0)} n_{\mathrm{BE}}(\bar{\omega})\right) = G_n^<(\omega-\omega_0)\mathcal{A}(\omega_0) + \int \frac{d\hbar\bar{\omega}}{2\pi}\frac{\delta G^<(\omega-\bar{\omega})}{\delta f(\omega_0)}\mathcal{A}(\bar{\omega}) n_{\mathrm{BE}}(\bar{\omega}),$$

$$\frac{\delta\Sigma_c^>(\omega)}{\delta f(\omega_0)} = G_n^>(\omega-\omega_0)\mathcal{A}(\omega_0) + \int \frac{d\hbar\bar{\omega}}{2\pi}\frac{\delta G^>(\omega-\bar{\omega})}{\delta f(\omega_0)} \times \mathcal{A}(\bar{\omega})[1+n_{\mathrm{BE}}(\bar{\omega})], \quad (29)$$

where the propagator terms are related to them by the relationship[30]

$$\frac{\delta\Sigma_c^{r,a}(\omega)}{\delta f(\omega_0)} = \frac{1}{2\pi}\int \frac{d\bar{\omega}}{\omega-\bar{\omega}\pm i\delta}\left(\frac{\delta\Sigma_c^>(\bar{\omega})}{\delta f(\omega_0)} + \frac{\delta\Sigma_c^<(\bar{\omega})}{\delta f(\omega_0)}\right). \quad (30)$$

If these expressions are substituted in Eq. (26), the closed set of linearized transport equations can be obtained in the form [equation for $\delta G^>(\omega)/\delta f(\omega_0)$ is analogous]

$$\frac{\delta G^<(\omega)}{\delta f(\omega_0)} = \int \frac{d\bar{\omega}}{2\pi} 2\mathrm{Re}\left(\frac{G_n^r(\omega)G_n^<(\omega)}{\omega-\bar{\omega}+i\delta}\frac{\delta\Sigma_H^r}{\delta f(\omega_0)}\right) + \int \frac{d\bar{\omega}}{2\pi} 2\mathrm{Re}\left(\frac{G_n^r(\omega)G_n^<(\omega)}{\omega-\bar{\omega}+i\delta}\right)\left[A_n(\bar{\omega}-\omega_0)\mathcal{A}(\omega_0) + \int \frac{d\hbar\bar{\bar{\omega}}}{2\pi}\left(\frac{\delta G^<(\bar{\omega}-\bar{\bar{\omega}})}{\delta f(\omega_0)}\mathcal{A}(\bar{\bar{\omega}}) n_{\mathrm{BE}}(\bar{\bar{\omega}}) + \frac{\delta G^>(\bar{\omega}-\bar{\bar{\omega}})}{\delta f(\omega_0)}\mathcal{A}(\bar{\bar{\omega}})[1+n_{\mathrm{BE}}(\bar{\bar{\omega}})]\right)\right] + |G_n^r(\omega)|^2\left(G_n^<(\omega-\omega_0)\mathcal{A}(\omega_0) + \int \frac{d\hbar\bar{\omega}}{2\pi}\frac{\delta G^<(\omega-\bar{\omega})}{\delta f(\omega_0)}\mathcal{A}(\bar{\omega}) n_{\mathrm{BE}}(\bar{\omega})\right). \quad (31)$$

The first term on the right side is the Hartree contribution. The remaining terms can be divided into terms representing the nonvertex solution (terms without functional derivative) and vertex corrections.

Equations (31) can substitute a *phono* Kubo formula, in analogy to the linearized transport equations in weak electric fields.[30,35] They are valid for interaction strengths going beyond the validity regime of the Boltzmann equation. A phono conductivity can be defined as a current response induced by a unit change of population in a monoenergetic beam of phonons.[5] It can be calculated from the linearized version of the formula (22) with the solutions in Eq. (31),

$$\frac{\delta J}{\delta f(\omega_0)} = \frac{e}{2}\int \frac{d\bar{\omega}}{2\pi}\left\{ [\Gamma_L^<(\bar{\omega}) - \Gamma_R^<(\bar{\omega})]\frac{\delta A(\bar{\omega})}{\delta f(\omega_0)} - [\Gamma_L^>(\bar{\omega}) + \Gamma_L^<(\bar{\omega}) - \Gamma_R^>(\bar{\omega}) - \Gamma_R^<(\bar{\omega})]\frac{\delta G^<(\bar{\omega})}{\delta f(\omega_0)}\right\}. \quad (32)$$

The total monochromatic response results by subtraction of the solutions of Eq. (32) for the positive and negative frequencies. For a wider phonon distribution, integration over the phonon distribution can be performed.

V. NUMERICAL RESULTS AND DISCUSSIONS

Here we present numerical results of the hot-phonon-induced change in spectra, populations, and currents for the present tunneling system.

A. Simple approach to the induced spectra

Some predictions about the hot-phonon-induced response results already from a simplified analysis. Let us limit to the study of the spectral changes.

1. Single-level system

To understand the hot-phonon-induced change of the spectrum, consider that the homogeneously broadened spectral function $A_{\mathrm{cold}}(\omega)$ is of the Lorentzian form (equilibrium phonons are neglected)

$$A_{\mathrm{cold}}(\omega) = -2\mathrm{Im}\left(\frac{1}{\hbar\omega - E_0 + i\sigma_{\mathrm{hom}}}\right) \quad (33)$$

and the electron population is low $n_{FD}\to 0$.

This system is irradiated by a monochromatic phonon beam of a population $\delta f(\omega)$ in Eq. (24) [$\delta f(\omega)=\Delta, \omega=\omega_0$]. The lowest order of perturbation theory gives the change of the self-energy

$$\Delta\Sigma_c^r(\omega)\approx\Delta(M\omega_0)^2\int\frac{d\hbar\bar{\omega}}{2\pi}\frac{A_{\rm cold}(\bar{\omega}-\omega_0)+A_{\rm cold}(\bar{\omega}+\omega_0)}{\omega-\bar{\omega}+i\delta}, \tag{34}$$

where the hot-phonon emission and absorption processes are represented by the shifts $\pm\omega_0$. The hot spectral function $A_{\rm hot}(\omega)$ results from Eq. (33) by the substitution $i\sigma_{\rm hom}\rightarrow i\sigma_{\rm hom}-\Delta\Sigma_c^r(\omega)$. At low phonon energies $\hbar\omega_0\ll\sigma_{\rm hom}$, the shifted functions $A_{\rm cold}(\omega\pm\omega_0)$ coincide in Eq. (34), which leads only to additional broadening of the Lorentzian $A_{\rm cold}(\omega)$ (as in elastic scattering). Therefore this transport regime can be called *quasielastic*. The maxima of the change $A_{\rm hot}(\omega)-A_{\rm cold}(\omega)$ appear close to the inflection points of $A_{\rm cold}(\omega)$, so that their distance is much larger than the phonon energy. For higher phonon energies $\hbar\omega_0>\sigma_{\rm hom}$, the broadening has a character of satellites in $A_{\rm hot}(\omega)$, which shift linearly with $\hbar\omega_0$. In experiments[8] the separation of the induced current peaks is much bigger than the phonon energy, as in the above quasielastic regime, and depends only slightly on temperature.

2. Many-level system

Similar behavior can be observed if the spectral function $A_{\rm cold}$ is dominated by the *inhomogeneous* broadening $\sigma_{\rm inh}$,[37] originating from different neighborhoods of many impurities in the system. The level distribution can be represented by a Gaussian law

$$f_i(E)=\frac{1}{\sigma_{\rm inh}\sqrt{2\pi}}\exp\left(-\frac{(E-E_0)^2}{2\sigma_{\rm inh}^2}\right), \tag{35}$$

where E_0 is the average level energy. Perturbation of this system of narrow levels by a weak monochromatic phonon field with the frequency ω_0 induces a change of the total spectral function $[\Omega=(\hbar\omega-E_0)/\sigma_{\rm inh}\sqrt{2},\quad \Omega_0=\hbar\omega_0/\sigma_{\rm inh}\sqrt{2}]$

$$\begin{aligned}A_{\rm hot}(\Omega)-A_{\rm cold}(\Omega)\approx\frac{\delta}{\sigma_{\rm inh}}\{&-2\exp(-\Omega^2)\\&+\exp[-(\Omega-\Omega_0)^2]\\&+\exp[-(\Omega+\Omega_0)^2]\},\end{aligned} \tag{36}$$

where the perturbation strength is again $\delta=\Delta(M\omega_0)^2$. The expression (36) has two local maxima in the positions $\pm\Omega_{\rm max}$.

In Fig. 2 we show the dependence of $\log_{10}(\Omega_{\rm max})$ on $\log_{10}(\Omega_0)$. For small phonon energies $\Omega_0<1$, only broadening of the Gaussian peak again takes place, with the maxima close to its inflection points ($\Omega_{\rm max}\approx1.6$). Here the emission (absorption) processes broaden the resonance only below (above) the main resonance, while for homogeneous broadening above, each of the processes broadens it at both sides, as $\Omega_0\rightarrow0$. For larger phonon energies $\Omega_0>1$, satellites are formed with maxima located at $\Omega_{\rm max}\approx\Omega_0$. In the inset we show the relative magnitude of the maximum of $[A_{\rm hot}(\omega)-A_{\rm cold}(\omega)]\sigma_{\rm hom}/\delta$. For larger phonon energies $\Omega_0>1$, this maximum is approximately equal to 1, and for energies $\Omega_0<1$, it sharply falls down. Therefore the sensitivity to excitations is also very small.

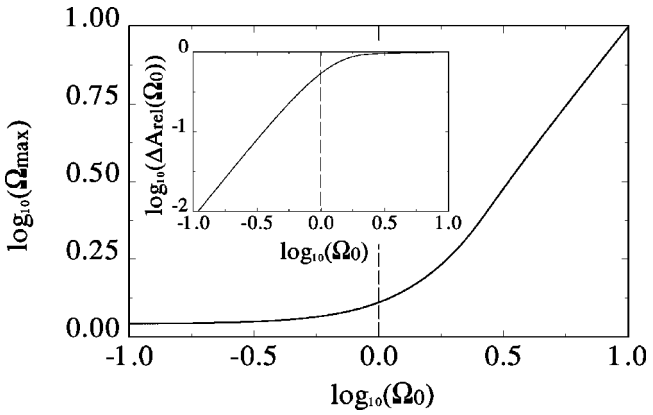

FIG. 2. The dependence of the maximum $\Omega_{\rm max}$ on the relative phonon energy Ω_0. In the inset the difference $[A_{\rm hot}(\omega)-A_{\rm cold}(\omega)]\sigma_{\rm inh}/\delta$ is shown as a function of Ω_0. For $\Omega_0<1$, formation of a quasielastic transport regime can be seen.

B. General approach to the induced spectra

Here we calculate, from the KB equations (5), the nonequilibrium spectra and distributions for some typical model parameters

1. Single-level system

In realistic structures the emitter band is weakly populated and the resonant level is comparably strongly coupled to both leads. This is modeled by $E_{F_L}=\mu_L-E_{{\rm bot};L}=1$ meV and $\gamma_L=7$ meV, $\gamma_R=5$ meV, giving in equilibrium $\sigma_{\rm hom}\approx2$ meV. Further parameters are $E_0=20$ meV, $T=1$ K and $T_h=1$ K (hot phonons are absent). In Fig. 3 we present the spectral $A(\omega)$ and correlation $G^<(\omega)$ functions

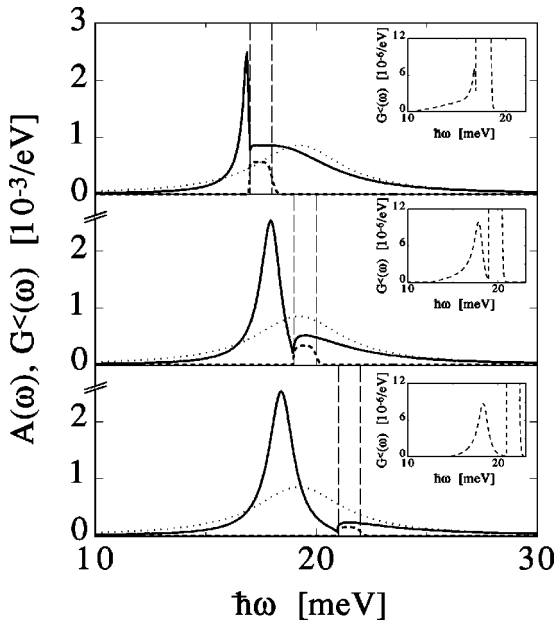

FIG. 3. The nonequilibrium (equilibrium) $A(\omega)$, shown by the solid (dotted) lines, and the nonequilibrium $G^<(\omega)$ (dashed lines) for the level position $E_0=20$ meV and the dc biases $\mu_L=-\mu_R=18,\ 20,\ 22$ meV (top to bottom). Below the injection windows (thin vertical dashed lines) $A(\omega)$ becomes larger and increases phonon emissions. The relaxed population in $G^<(\omega)$ copying $A(\omega)$ is presented in the insets.

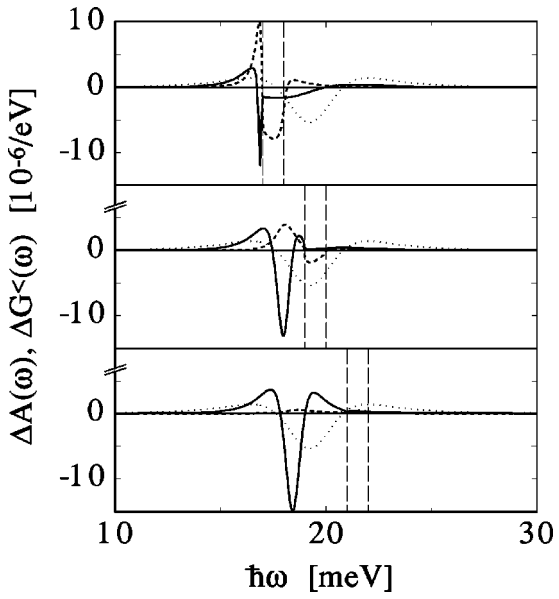

FIG. 4. The hot-phonon-induced nonequilibrium (equilibrium) $\Delta A(\omega)$ and nonequilibrium $\Delta G^{<}(\omega)$ for the parameters and solutions as in Fig. 3 [equilibrium $\Delta A(\omega)$ and nonequilibrium $\Delta G^{<}(\omega)$ are magnified by 4]. The narrowing of $\Delta A(\omega)$ below the injection window is seen, where the population in $\Delta G^{<}(\omega)$ relaxes by stimulated emissions.

under dc biases near the resonance $\mu_L=-\mu_R=18$, 20, 22 meV. The pairs of thin vertical dashed lines show the injection windows determined by $E_{\mathrm{bot};L}$ and μ_L. The solid (dotted) line represents the nonequilibrium (equilibrium, $\mu_L=\mu_R$) $A(\omega)$ and the short dashed line the nonequilibrium $G^{<}(\omega)$. As the emitter band moves up, its overlap with the level decreases and so does the effective coupling to the level. Therefore the nonequilibrium $A(\omega)$ becomes narrower (σ_{hom} smaller) but larger (density of states on the level increases). Moreover, the level moves down due to repulsion by the moving bands (emitter). The polaron shift of the level by the Hartree term (14) and the many-particle shift[38] are negligible here. The electrons injected on the level relax by phonon emissions below the bottom edge of the emitter band $E_{\mathrm{bot};L}$, where the increased density of states $A(\omega)$ further accelerates this scattering. In the insets magnified details of $G^{<}(\omega)$ reveal this relaxed electron population on the level, which contributes in the second term of the current formula (23).

Analogous effects become induced by the hot phonons. In Fig. 4 we show the subtracted functions $\Delta A(\omega)$ and $\Delta G^{<}(\omega)$, calculated for the phonon distribution $f_P(\omega)$ in Eq. (13) with $T_h=10$ K, $T=1$ K, and $T_h=T=1$ K (no hot phonons). Electrons in the leads remain at $T=1$ K and other parameters are as before. The same lines are used; the equilibrium ($\mu_L=\mu_R$)$\Delta A(\omega)$ and nonequilibrium $\Delta G^{<}(\omega)$ are magnified by 4. The two peaks in $\Delta A(\omega)$ result from the hot-phonon-induced broadening of $A(\omega)$, as in the quasielastic regime discussed in the preceding subsection [peaks are closer for narrower $A(\omega)$]. The presence of this regime is also confirmed by the fact that $k_{Bol}T_h\approx 1$ meV$<\sigma_{\mathrm{hom}}\approx 1-2$ meV. The relaxed population below $E_{\mathrm{bot};L}$ can be again observed in $\Delta G^{<}(\omega)$. Resolution into components shows that this part originates by phonon emissions, while the part above μ_L is due to phonon absorptions. Their amplitudes are again determined by the values of $A(\omega)$. The phonon-induced signal from spontaneous decay processes is one order of magnitude stronger than that from stimulated processes induced by phonons heated by a few degrees K.

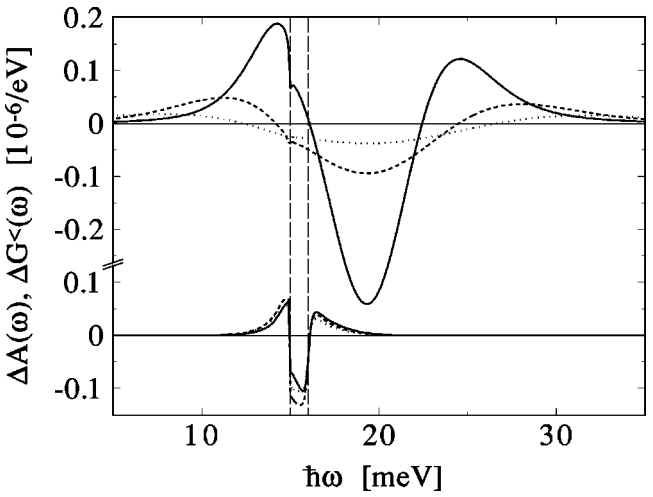

FIG. 5. The hot-phonon-induced $\Delta A(\omega)$ (upper drawing) and $\Delta G^{<}(\omega)$ (lower drawing) calculated for the many-level system and parameters as in the one-level model ($\gamma_L=5$ meV, $\gamma_R=7$ meV, and $\mu_L=18$ meV). The solutions for the width $\sigma_{\mathrm{inh}}=2$, 4, 6 meV are drawn by the solid, dashed, and dotted lines. $\Delta A(\omega)$ decreases and widens with σ_{inh}, while $\Delta G^{<}(\omega)$ remains nearly unchanged.

2. Many-level system

In Fig. 5 we present also $\Delta A(\omega)$ (upper diagram) and $\Delta G^{<}(\omega)$ (lower diagram) for a system with many levels distributed by Eq. (35) and the width $\sigma_{inh}=2$, 4, 6 meV (solid, dashed, and dotted lines). The other parameters are $\gamma_L=5$ meV, $\gamma_R=7$ meV, giving smaller populations of the level, and $\mu_L=18$ meV. As σ_{inh} increases, the separation between the peaks in $\Delta A(\omega)$ increases and their amplitude decreases, because contributions to $\Delta A(\omega)$ from different levels (oscillating in values; see Fig. 4) are shifted and cancel out. Since the broadening is predominantly inhomogeneous ($\sigma_{\mathrm{inh}}>\sigma_{\mathrm{hom}}\approx 2$ meV), $\Delta A(\omega)$ does not change considerably below $E_{\mathrm{bot};L}$. The solutions for $\Delta G^{<}(\omega)$ are very similar in value, because contributions from individual levels to $\Delta G^{<}(\omega)$ are all located around the common injection window and cancel much less. The decrease of the amplitude of $\Delta A(\omega)$ increases the importance of the relaxation term with $\Delta G^{<}(\omega)=A(\omega)\ \Delta f(\omega)$ in the current formula (23). Therefore the hot-phonon-induced two-peak structure from $\Delta A(\omega)$ becomes substituted in Eq. (23) by a single-peak profile of $\Delta f(\omega)$ [the density of states $A(\omega)$] below $E_{\mathrm{bot};L}$.

C. Induced *I-V* characteristics

We calculate the resonant current and its hot-phonon-induced change by substituting the above solutions for $A(\omega)$, $G^{<}(\omega)$, and $\Delta A(\omega)$, $\Delta G^{<}(\omega)$ in the formula (23).

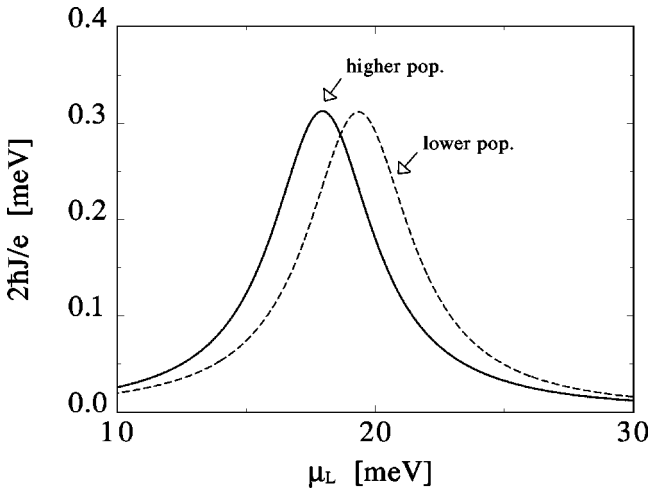

FIG. 6. The total *I-V* characteristics, calculated for the parameters in Fig. 3. The current for the higher populated solution is shifted to lower energies, due to a stronger repulsion by the emitter.

1. Single level system

In Fig. 6 we present the *I-V* characteristics for the solutions in Fig. 3 and the dc bias 10 meV$<\mu_L=-\mu_R<$30 meV. Two polarities of the dc bias used in experiments[8,20] are simulated here by two sets of coupling parameters, giving different level populations, $\gamma_L=7$ meV, $\gamma_R=5$ meV (solid line) and $\gamma_L=5$ meV, $\gamma_R=7$ meV (dashed line). The resonance peak results when electrons in the narrow populated emitter become injected in the level ($E_{F_L}\approx\sigma_{\rm hom}$). Both solutions are shifted down, since the free-level position $E_0=20$ meV is repelled by the moving bands.

In Fig. 7 the hot-phonon-induced current ΔJ is shown (solid line) for the solutions in Fig. 4 and coupling in Fig. 6. In the lower population mostly the first term in Eq. (23) contributes to ΔJ, which reflects the double peak in $\Delta A(\omega)$ [equilibrium $\Delta A(\omega)$ in Fig. 4 could be considered, since

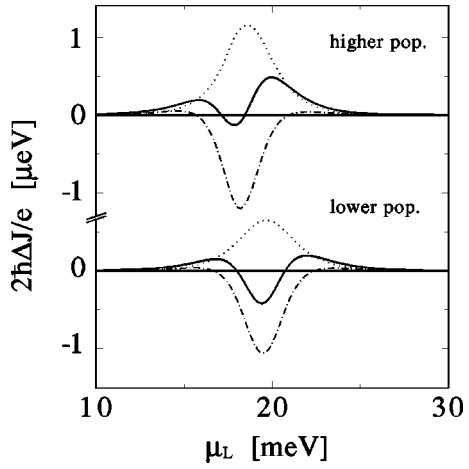

FIG. 7. The current ΔJ induced by hot phonons ($T_h=10$ K, $T=1$ K) for the parameters in Fig. 6 (solid lines). The elastic (thin dot-dashed lines) and inelastic (thin dotted lines) components are also presented. The more populated solution is distorted, because of the enhanced emission processes on the level (shifted and increased inelastic component).

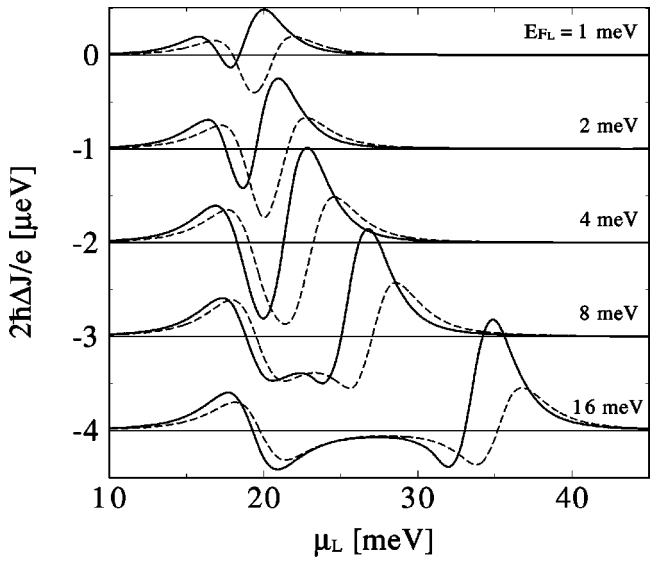

FIG. 8. The hot-phonon-induced current ΔJ for the parameters in Fig. 7 and the Fermi level $E_{F_L}=1,\ 2,\ 4,\ 8,\ 16$ meV (successive curves are displaced by -1 μeV). The solid (thin dashed) lines correspond to the higher (lower) populations. For $E_{F_L}>2\sigma_{\rm hom}=4$ meV the negative minimum splits.

$\gamma_L<\gamma_R$]. In the higher population the second (relaxation) term in Eq. (23) modifies the induced current to an asymmetric form with a smaller negative minimum. This deformation results because the elastic ΔJ_e (thin dot-dashed lines) and inelastic ΔJ_i (thin dotted lines) components of the total induced current are shifted. Resolution of $\Delta J_{e,i}$ into emission and absorption components clarifies this shift and the different size of ΔJ_i in both solutions. First the absorption components are shifted about 1 meV down with respect to the emission ones, because the transport is not fully in the quasielastic regime mentioned at Eq. (34). Second, in the higher population the inelastic emission component is two times bigger than in the lower population, but the other components are the same.

To summarize, we can say that the asymmetry of the induced tunneling current in the higher populated case is a manifestation of the relaxation term in Eq. (23), which is large due to the following facts.

(1) Stronger emitter coupling $\gamma_L>\gamma_R$ gives larger level populations $f(\omega)[G^<(\omega)]$, so the relaxation term in Eq. (23) can be important.

(2) $f(\omega)$ reflects in Eq. (23) only electrons relaxed by phonon emissions below the injection window (seen in Fig. 4).

(3) In this region the density of final states $A(\omega)$ is reasonably increased (coupling by γ_L is absent), so the emission processes are stronger.

The enhanced *intralevel* phonon emissions invalidate transmissivity approaches, which neglect electron relaxation during the tunneling. Similar asymmetry of the current response has also been observed in experiments.[8,9,20]

In Fig. 8 we present the induced current for different emitter populations $E_{F_L}=1,\ 2,\ 4,\ 8,\ 16$ meV, realized by shifting the equilibrium value $E_{{\rm bot};L}=-E_{F_L}$. The solid (thin dashed) lines correspond to the stronger (lower) filling of the level for $\gamma_L=7$ meV and $\gamma_R=5$ meV ($\gamma_L=5$ meV and

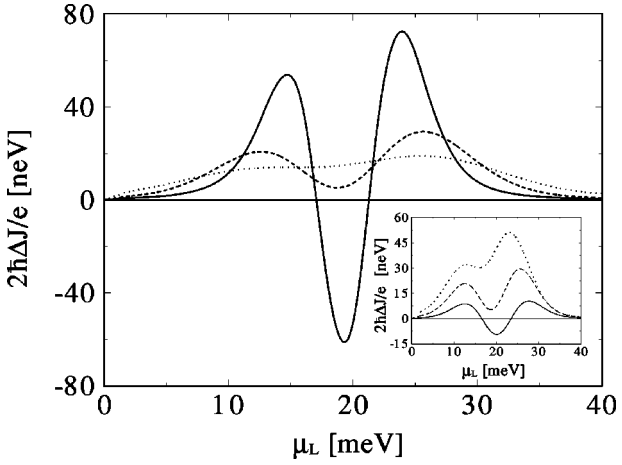

FIG. 9. The hot-phonon-induced current ΔJ, calculated for parameters in Fig. 5 and drawn by the same lines. The change of form results from the current formula (23), where the two-peak structure in ΔA is substituted by the resonance form of $\Delta f(A)$. In the inset the coupling is varied $\gamma_L = 3,\ 5,\ 7$ meV (solid, dashed, and dotted lines) for the solution with $\sigma_{\rm inh} = 4$ meV.

$\gamma_R = 7$ meV). The amplitude of ΔJ increases with E_{F_L} up to the value $E_{F_L} \approx 4$ meV, where the populated region of the emitter approximately covers the whole resonance $E_{F_L} \approx 2\sigma_{\rm hom}$ and ΔJ saturates. If E_{F_L} further increases, the negative peak splits into two minima and the negative flat values in the midle approach zero.

2. Many-level system

In Fig. 9 the induced current ΔJ is found for $\Delta A(\omega)$ in Fig. 5, with the inhomogeneous broadening $\sigma_{\rm inh} = 2,\ 4,\ 6$ meV (solid, dashed, and dotted lines). We can see a transfer from a double to a single (wider) peak form, due to the transfer of a dominance from the injection to the relaxation term in the formula (23), as described in Fig. 5. In the inset we also show ΔJ as a function of the coupling $\gamma_L = 3,\ 5,\ 7$ meV (solid, dashed, and dotted lines), $\sigma_{\rm inh} = 4$ meV, and other parameters unchanged. As γ_L increases, similar changes are observed (faster than in Fig. 7, since $\sigma_{\rm inh} > 0$).

3. Monochromatic phono response

We present the current induced by monochromatic phonon excitations. The response is normalized to the increase of population $n_{\rm noneq} = 1$ in the energy interval 1 meV. Both the nonlinear (5) and the linearized methods (31) give very close results here.

The current for the single-level model is shown in Fig. 10 for the parameters in Fig. 7, the excitation phonon energy $\hbar\omega_0 = 1$–6 meV, and the coupling $\gamma_L = 7$ meV, $\gamma_R = 5$ meV. For low phonon energies $\hbar\omega_0 \to 0$, the quasielastic regime [discussed at Eq. (34)] is maintained and the positions of the positive peaks saturate close to the inflection points of the resonance (here each of the two peaks has both emission and absorption components). As $\hbar\omega_0 > \sigma_{\rm hom} = 2$ meV, the system leaves the quasielastic regime and the two peaks can be solely attributed to phonon absorption (left peak) and emission (right peak). In this region the positions

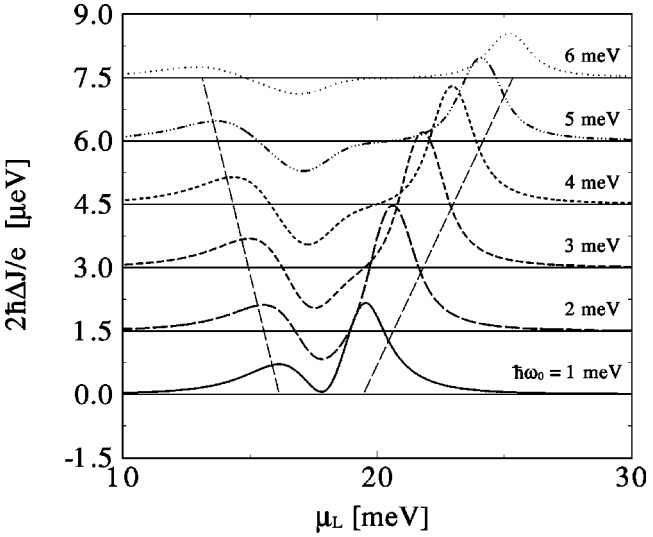

FIG. 10. The induced current ΔJ for the single-level model, monochromatically excited with energies $\hbar\omega_0 = 1$–6 meV (curves are displaced by 1.5 μeV). The coupling is $\gamma_L = 7$ meV, $\gamma_R = 5$ meV. The position of the maxima (thin dashed lines) shifts linearly with $\hbar\omega_0$ and their amplitude falls as $\hbar\omega_0$ grows.

of the maxima, denoted by thin dashed lines, shift approximately linearly with the phonon energy and the amplitudes of the peaks saturate. The right (emission) peak increases in size even at higher $\hbar\omega_0$ and makes the response very asymmetric, due to population effects on the level for this coupling $\gamma_L > \gamma_R$. As $\hbar\omega_0 > 5$ meV, the size of both peaks rapidly falls, because a cutoff is imposed on the excitation energies by the confinement of the level in the quantum well; i.e., the factor $F(q)$ in Eq. (3) is approximately localized within a range $|\Delta q_z| \approx 2\pi/w$. This gives the limiting excitation energy $\hbar\omega_{\rm lim} \approx \hbar s \Delta q_z = 4.3$ meV [$\hbar\omega_{\rm lim} \approx 6.5$ meV, if all three terms in $F(q)$ are taken into account].

These results can be compared with Fig. 11, calculated for the same parameters, but for excitations by the hot-phonon

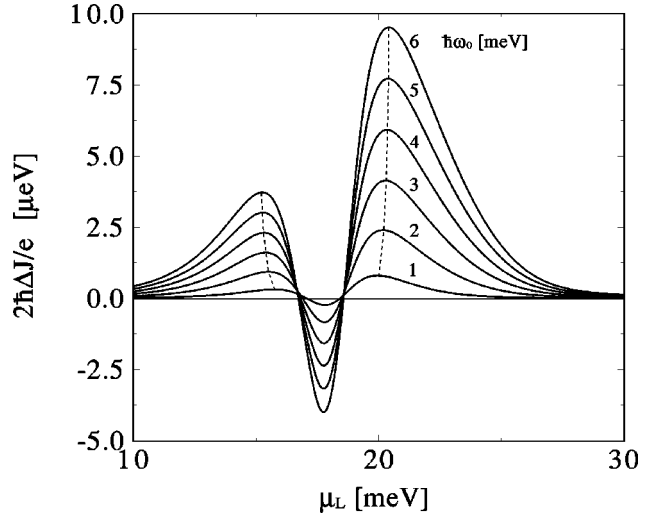

FIG. 11. The induced current ΔJ excited by hot phonons with temperature $k_B T_h = \hbar\omega_0 = 1$–$6$ meV. In contrast to Fig. 10, the positions of the peaks shift very little and the amplitude remains growing with $k_B T_h = \hbar\omega_0$, since only low frequency phonons (in the tail) can excite the level.

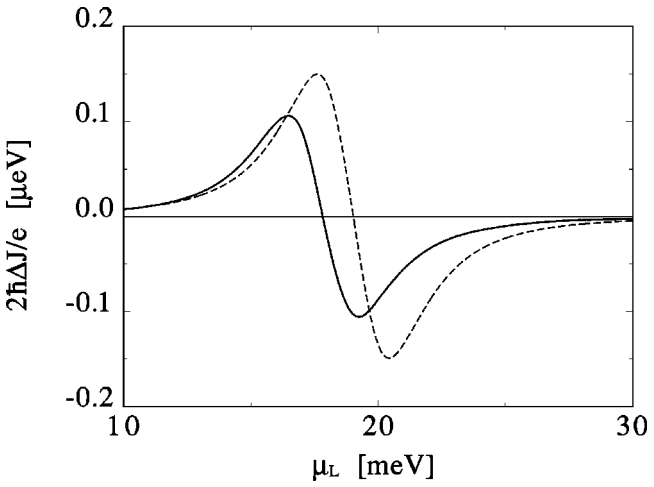

FIG. 12. The current response ΔJ induced by heating the electrons in the leads from $T_e=1$ K to $T_e=1.1$ K (phonons are at $T=1$ K). The solid (weak dashed) line corresponds to $\gamma_L=7$ meV, $\gamma_R=5$ meV ($\gamma_L=5$ meV, $\gamma_R=7$ meV). The solutions have a different symmetry than in Fig. 7 but the response is much stronger for a small heating of the electrons in the reservoir.

distribution (13) of the temperature equal to the previous energies $k_B T_h=\hbar\omega_0=1$–6 meV (12–70 K). At low temperatures, the peaks (thin dashed line) shift slightly as the phonon energy increases. At high temperatures their position saturates, because the maximum of $f_P(\omega)$ is located at higher energies than the cutoff $\hbar s\Delta q_z$ and only the low frequency tail of $f_P(\omega)$ falls in this region (experiments give similar behavior.[8]) On the other hand, the population increase with T_h, in this low frequency tail, gives the increase of the response signal in Fig. 11. The amplitude of the peaks varies as $\approx T_h^2$, similarly as in a simple heating of the electrons in the leads, discussed below.

D. Heating of the electron gas

In the above calculations ΔJ results only from the hot-phonon-assisted processes. In experiments electrons in the leads $[f_{L,R}(\omega)]$ are also heated to some extent by nonequilibrium phonons. Moreover, measurements performed without the hot-phonon injection[20] (current is subtracted for two different temperatures of the system) give very similar difference currents. In this case heating of the leads cannot be avoided.

To appreciate these effects, we calculate in Fig. 12 the difference in current resulting from heating of the electrons in the reservoirs. Here they are heated to $T_e=1.1$ K, all phonons are $T=1$ K, and the other parameters are as in Fig. 7. The solid (weak dashed) line represents the coupling $\gamma_L=7$ meV, $\gamma_R=5$ meV ($\gamma_L=5$ meV, $\gamma_R=7$ meV). The response reflects redistribution of electrons in the emitter (the zero value coincides with the position of the resonance in Fig. 6), so that its form is different from the phonon-assisted signal in Fig. 7. For electrons heated only about 10%, the response amplitude is of the same order as in Fig. 7, where phonons are heated to 10 K. In the experiments without hot phonons, the ratio $\Delta J/J$ is also one to two orders stronger than the theoretical predictions for the phonon-assisted signal and rather corresponds to this heating amplitude.[20] On the other hand, the *form* of the experimental response agrees well with the phonon-assisted tunneling in Fig. 7. This means that experiments cannot be explained by the simple heating.

One possibility for explanation of these differences is to assume that our model is oversimplified. It can be, for example, improved by considering that the planar emitter is formed by a system of dots, located around each charged impurity in the well. Their discrete level character could prevent direct heating of the tunneling electrons and can also increase the strength of the electron-phonon interaction.[19]

VI. CONCLUSION

We have theoretically studied dc resonant tunneling of electrons through an impurity level in a quantum well, assisted by heated acoustic phonons coupled to electrons on the level. The transport was analyzed in terms of the hot-phonon-induced change in the spectrum and distribution of electrons on the level, reflected in the tunneling current. The current formulas have been clearly divided in the injection and relaxation parts, where the roles of the spectrum and population of the level are separated.

Several transport regimes have been identified. The induced change in the spectra and currents is given by two peaks separated by a minimum. For low energy phonons, the peaks correspond to a phonon-induced level broadening and the transport can be considered as quasielastic. For high energy phonons, true satellite peaks are induced in both functions. If the level is more strongly coupled to the emitter, intralevel phonon emissions are enhanced and the current response results distorted by the population of the electrons relaxed below the injection region. This intralevel relaxation can completely change the induced response, especially in the presence of inhomogeneous broadening. Our calculations qualitatively agree with the experimental observations. We believe that this study improves general understanding of inelastic processes assisting resonant tunneling.

ACKNOWLEDGMENTS

This work has been supported by NATO and the Royal Society. The authors would like to thank L. J. Challis and A. V. Akimov for many stimulating discussions.

APPENDIX

The causal fermion ($O=\psi$) or boson ($O=A$) Green functions in real times are defined by[29] (Matsubara Green functions are analogous)

$$G^t(1,2)=-\frac{i}{\hbar}\langle T[O(1)O^\dagger(2)]\rangle, \quad j\equiv(r_j,t_j), \quad (j=1,2). \tag{A1}$$

They are related to the correlation functions as follows:

$$i\hbar G^t(1,2)=G^>(1,2)=\langle O(1)O^\dagger(2)\rangle, \quad t_1>t_2$$
$$\mp i\hbar G^t(1,2)=G^<(1,2)=\langle O^\dagger(2)O(1)\rangle, \; t_1<t_2, \tag{A2}$$

where the upper (lower) sign applies to fermions (bosons). The retarded and advanced Green functions are defined by

$$G^r(1,2) = -\frac{i}{\hbar}\theta(1-2)[G^>(1,2) \pm G^<(1,2)],$$

$$G^a(1,2) = \frac{i}{\hbar}\theta(2-1)[G^>(1,2) \pm G^<(1,2)], \quad \text{(A3)}$$

where the time step is $\theta(t)=0,\ t<0;\ \ \theta(t)=1,\ t\geqslant 0$.

In steady-state situations a Fourier transform over the difference of coordinates $(r,t)=(r_1-r_2,t_1-t_2)$ gives fermion and boson correlation functions[10]

$$G^<(k,\omega) = n_{F,B}(\hbar\omega)A(k,\omega),$$

$$G^>(k,\omega) = [1 \mp n_{F,B}(\hbar\omega)]A(k,\omega), \quad \text{(A4)}$$

where n_F, n_B denote the Fermi-Dirac and Bose-Einstein distributions and the spectral function is defined by

$$A(k,\omega) = -2\,\mathrm{Im}\,G^r(k,\omega) = G^>(k,\omega) \pm G^<(k,\omega). \quad \text{(A5)}$$

The retarded Green function can be calculated from the spectral function (A5) by the Hilbert transform

$$G^r(k,\omega) = \int_{-\infty}^{\infty} \frac{d\overline{\omega}}{2\pi} \frac{A(k,\overline{\omega})}{\omega - \overline{\omega} + i\delta}. \quad \text{(A6)}$$

Similar formulas can be applied also for the self-energy.

*Permanent address: Institute of Physics, Academy of Sciences, Na Slovance 2, 180 40 Praha 8, Czech Republic.

[1] L. J. Challis, A. J. Kent, and V. W. Ramp, Semicond. Sci. Technol. **5**, 1179 (1990).

[2] J. K. Wigmore, K. R. Strickland, S. C. Edwards, and A. R. Collins, in *Phonon Scattering in Condensed Matter VII*, edited by M. Meissner and R. P. Pohl (Springer-Verlag, New York, 1993), pp. 279–280; M. Giltrow *et al.*, Phys. Rev. Lett. **75**, 1827 (1995).

[3] C. J. Mellor, R. H. Eyles, J. E. Digby, A. J. Kent, K. A. Benedict, L. J. Challis, M. Henini, C. T. Foxon, and J. J. Harris, Phys. Rev. Lett. **74**, 2339 (1995).

[4] A. J. Kent, R. E. Strickland, K. R. Strickland, and M. Henini, Phys. Rev. B **54**, 2019 (1996).

[5] M. Blencowe and A. Shik, Phys. Rev. B **54**, 13 899 (1996).

[6] V. J. Goldman, D. C. Tsui, and J. E. Cunningham, Phys. Rev. B **36**, 7635 (1987).

[7] V. I. Kozub and A. M. Rubin, Phys. Rev. B **47**, 13 737 (1993).

[8] F. F. Ouali, N. N. Zinov'ev, L. J. Challis, F. W. Sheard, M. Henini, D. P. Steenson, and K. R. Strickland, Phys. Rev. Lett. **75**, 308 (1995).

[9] F. F. Ouali *et al.*, Surf. Sci. **361/362**, 181 (1996).

[10] L. P. Kadanoff and G. Baym, *Quantum Statistical Mechanics* (Benjamin, New York, 1962).

[11] L. V. Keldysh, Zh. Éksp. Teor. Fiz. **47**, 1515 (1964) [Sov. Phys. JETP **20**, 1018 (1965)].

[12] C. Caroli, R. Combescot, P. Nozieres, and D. Saint-James, J. Phys. C **5**, 21 (1972).

[13] E. V. Ando and F. Flores, J. Phys.: Condens. Matter **3**, 9087 (1991).

[14] R. Lake and S. Datta, Phys. Rev. B **45**, 6670 (1992).

[15] C. H. Grein, E. Runge, and H. Ehrenreich, Phys. Rev. B **47**, 12 590 (1993).

[16] J. H. Davies, S. Hershfield, P. Hyldgaard, and J. W. Wilkins, Phys. Rev. B **47**, 4603 (1993).

[17] P. Hyldgaard, S. Hershfield, J. H. Davies, and J. W. Wilkins, Ann. Phys. (N.Y.) **236**, 1 (1994).

[18] P. Král and A. P. Jauho (unpublished).

[19] Ø. Lund Bø and Yu Galperin, J. Phys.: Condens. Matter **8**, 8595 (1996).

[20] P. Král, F. W. Sheard, F. F. Ouali, and L. J. Challis, Phys. Status Solidi B **204**, 438 (1997); D. N. Hill *et al.*, *ibid.* **204**, 431 (1997); P. Kral, F. W. Sheard, F. F. Ouali, D. N. Hill, A. V. Akimov, and L. J. Challis, Phys. Rev. E (to be published).

[21] F. W. Sheard and T. M. Fromhold, Acta Phys. Pol. A **82**, 523 (1992).

[22] G. D. Mahan, *Many Particle Physics* (Plenum, New York, 1981).

[23] V. Karpus, Fiz. Tekh. Poluprovodn. **22**, 439 (1988) [Sov. Phys. Semicond. **22**, 268 (1988)]; J. C. M. Henning *et al.*, Phys. Rev. B **53**, 15 802 (1996), and references therein.

[24] A. J. Kent *et al.*, Semicond. Sci. Technol. **12**, 849 (1997).

[25] D. C. Langreth, in *Linear and Nonlinear Electron Transport in Solids*, edited by J. T. Devreese and E. van Boren (Plenum, New York, 1976).

[26] A. P. Jauho, Phys. Rev. B **32**, 2248 (1985).

[27] E. N. Economou, in *Green's Functions in Quantum Physics*, Springer Series in Solid-State Sciences Vol. 7 (Springer, Berlin, 1979).

[28] A. B. Migdal, Zh. Éksp. Teor. Fiz. **34**, 1438 (1958) [Sov. Phys. JETP **7**, 996 (1958)].

[29] A. A. Abrikosov, L. P. Gorkov, and I. Y. Dzyaloshinski, *Quantum Field Theoretical Methods in Statistical Physics* (Pergamon Press, New York, 1965).

[30] P. Král, Phys. Rev. B **53**, 11 034 (1996).

[31] Y. Meir and N. S. Wingreen, Phys. Rev. Lett. **68**, 2512 (1992).

[32] R. Landauer, IBM J. Res. Dev. **1**, 223 (1957).

[33] N. S. Wingreen, K. W. Jacobsen, and J. W. Wilkins, Phys. Rev. B **40**, 11 834 (1989).

[34] F. Chevoir and B. Vinter, Phys. Rev. B **47**, 7260 (1993).

[35] M. P. Anantram and S. Datta, Phys. Rev. B **51**, 7632 (1995).

[36] G. Baym, Phys. Rev. **127**, 1391 (1962).

[37] Ch. P. Poole, Jr. and H. A. Farach, *Relaxation in Magnetic Resonance* (Academic Press, New York, 1971).

[38] P. Král, Phys. Rev. B **56**, 7293 (1997).